JOURNAL OF GEOPHYSICAL RESEARCH, VOL. 101, NO. C7, PAGES 16,667–16,682, JULY 15, 1996

Flow around a coastal bend: A model of the Santa Barbara Channel eddy

Lie-Yauw Oey

Program in Atmospheric and Oceanic Sciences, Princeton University, Princeton, New Jersey

Abstract. A steady, equatorward wind stress is applied over a two-layer ocean (infinitely deep lower layer) west of an otherwise straight meridional coast with a right-angle bend. Initial ($t \approx 10$ days) response consists of an equatorward current (Kelvin wave) that triggers a cyclone around the bend through viscous production and advection of vorticity, a process akin to eddy shedding in flows without rotation. The response at large times is governed by a Kelvin wave forced by the equatorward weakening of the (assumed positive) wind stress curl, which produces a poleward current near the coast. Application to the Santa Barbara Channel cyclone is discussed, and the cyclone-formation process is further demonstrated with a three-dimensional model with topography and stratification.

1. Introduction

This study was motivated by my attempt to numerically model the coastal ocean response along California under spring/summer condition when southward wind prevails. The reduced-gravity (1.5-layer) model I used shows (Figure 1) cyclonic eddies produced as flow negotiates around coastline bends. The process is ageostrophic ($\varsigma/f \approx 1$), and the cyclonic recirculation and upwelling features appear to have their counterparts in the observations, around Point Conception west of the Santa Barbara Channel (SBC), for example [*Brink and Muench*, 1986; *Lagerloef and Bernstein*, 1988]. This note discusses processes which affect cyclone formation around a coastal bend, the western SBC in particular.

2. The Model

The model is finite differenced (second order) on a C grid and leapfrogged in time and is governed by the following equations:

$$h_t + \nabla \cdot (h\mathbf{u}) = 0 \tag{1a}$$

$$\partial(\mathbf{u}h)/\partial t + \nabla \cdot [\mathbf{u}(\mathbf{u}h)] + fh\mathbf{k} \times \mathbf{u} = -g'h\nabla h + \tau^o + \nabla \cdot [\nu\nabla(h\mathbf{u})] + \nabla[\nu\nabla \cdot (h\mathbf{u})] \tag{1b}$$

where $\mathbf{u}$ is the horizontal velocity vector, h is the layer depth (with a specified undisturbed value $H = 100$ m), τ^o is the kinematic wind stress, ν is the viscosity coefficient, g' is the reduced gravity ($=10^{-2}$ m s^{-2}), and f is the constant Coriolis parameter at 34°N ($=8 \times 10^{-5}$ s^{-1}). The model has two viscous terms in (1b), but only the shear part from the first term is significant.

3. The Mechanics of Cyclone Formation

To isolate the process, we examine the flow along a straight coast with a single bend (the domain mimics SBC). Figure 2 shows a case with southward wind applied north of the bend and Figure 3 with southward wind applied everywhere. In the former the flow veers westward as it leaves the coast at the bend under the influence of the Coriolis force [c.f. *Narimousa and Maxworthy*, 1989]. In the latter a cyclone develops in the channel. Therefore the cyclone is produced by equatorward flow around the bend; the flow is in turn forced from the south. (As pointed out by one of the reviewers, the abrupt vanishing of the wind stress south of the bend (used in Figure 2) is unrealistic. However, the conclusion is unchanged when a gradual tapering is used (compare analysis in section 5).)

Experiments are conducted to examine which of the terms in the governing equation are responsible for cyclone formation. I choose a subdomain of Figure 2 that focuses on the channel only (Figure 4; note that north is now model's positive x direction), with $\Delta x = \Delta y = 1$ km and a relatively large value of $\nu = 40$ m^2/s. The forcing is an outflow velocity $v(x) = -v_o \exp(x/R_o)$ specified at $y = 0$, where $v_o = 0.2$ m s^{-1} and $R_o = 13$ km (the Rossby radius of deformation) and $\tau^o = 0$. Figure 4 shows the case with no-slip condition at the wall. Setting the advection terms in (1b) to zero results in no cyclone formation. On the other hand, a cyclone is produced when Coriolis is turned off (instead of the exponential variation, uniform inflow is specified at the upstream boundary; also, the left and top boundaries are free-slip walls). However, instead of a cyclone which quickly (5 days) becomes near stationary due to geostrophy (Figure 4), the cyclone in the case with zero Coriolis drifts into the channel as a new one is formed at the corner (Figure 5). The process is the same as eddy shedding behind a "bluff" body [*Batchelor*, 1967]. These experiments suggest that vorticity is produced at the corner through viscosity (not by vortex stretching) and advected into the channel.

That the corner vorticity arises can be understood by considering how a free-slip condition may be applied at the corner, so that vorticity production is nil. The vorticity along a curved boundary is $\varsigma = U/R - \partial U/\partial n$, where U is the speed of a fluid parcel following the boundary, n is positive to the left of the parcel's path, and R is the radius of curvature [*Gill*, 1982] (R is positive in the present case of flow that turns left around the corner). For the no-slip case (Figure 4) the model uses discontinuous values of ς at the corner [*Roache*, 1972]. For free slip a wall vorticity $\varsigma_w = 2U/R$ must be specified to compensate the corner vorticity [*Holloway and Rhines*, 1991], or $\partial U/\partial n|_{\text{wall}} = -U/R$. Since $R = 0^+$ at the corner, this condition cannot

Paper number 96JC01232.
0148-0227/96/96JC-01232$09.00

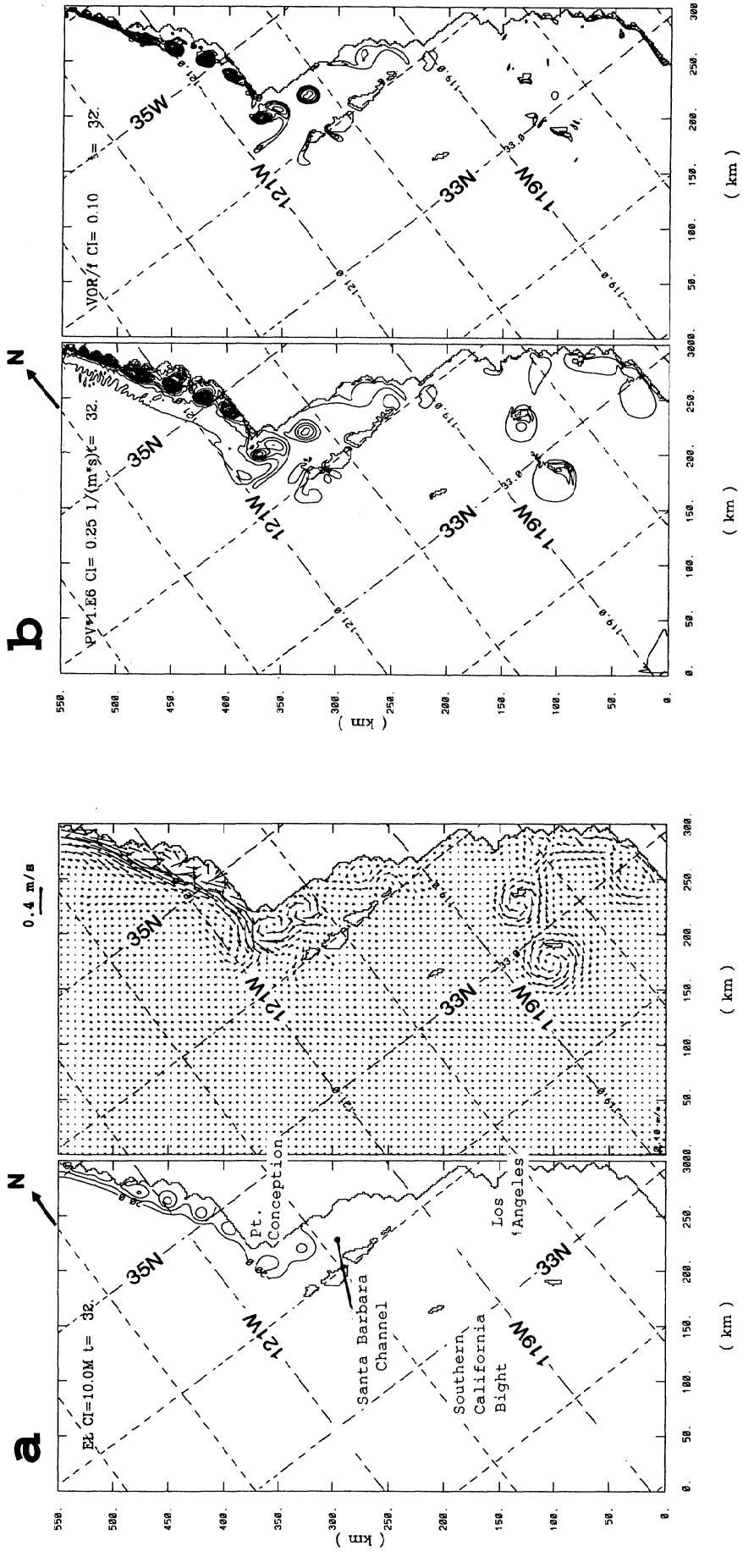

Figure 1. An example of (a) modeled layer anomaly ($=h - H$; contour interval (CI) is 10 m; plotted values are negative, i.e., decreased layer depth) and velocity vectors and (b) potential vorticity (CI = 2.5×10^{-7} 1/(meters $\times$ second)) and vorticity/f (CI = 0.1; plotted values are positive). Domain is from south to central California shelf and slope. Wind is southeastward $\tau^{oy} = -1.25 \times 10^{-4}$ m^2 s^{-2}. The grid sizes are $\Delta x = \Delta y = 5/3$ km, $\nu = 5$ m^2 s^{-1}, and the boundary conditions are radiation north and west, zero gradient at south, and no slip at coast.

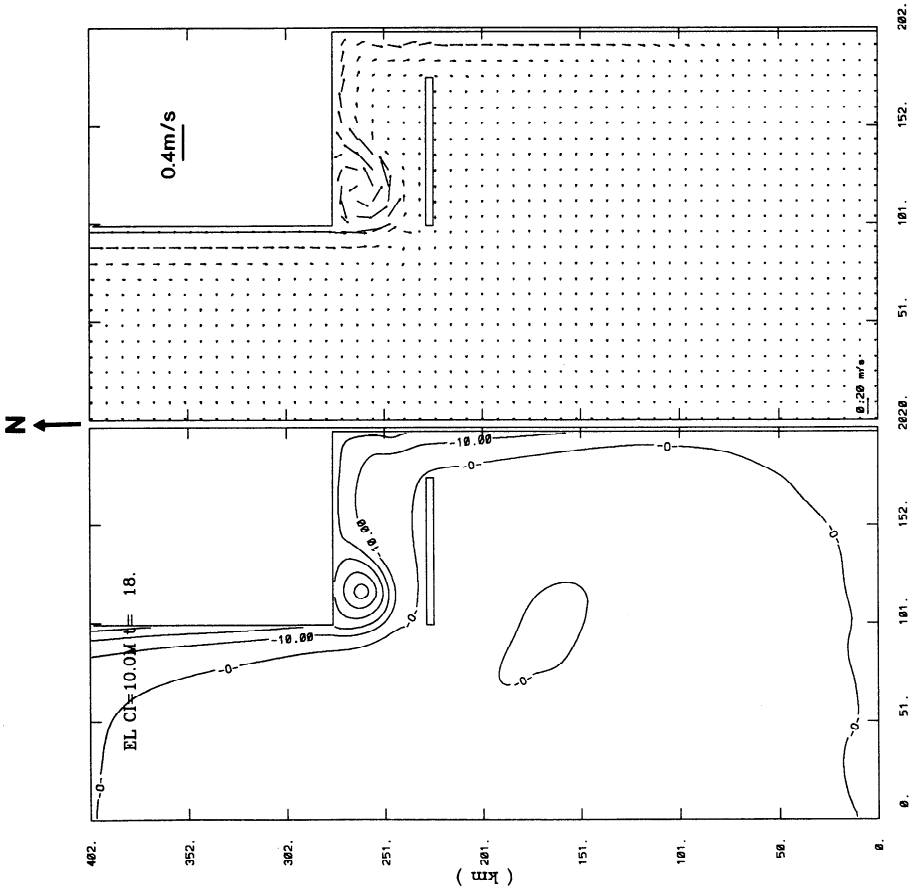

Figure 2. Modeled layer anomaly (CI = 10 m) and vectors in an idealized ocean with a single coastal bend and "Santa Barbara Channel." The wind was $\tau^{oy} = -2 \times 10^{-4}$ m^2 s^{-2} applied north of the bend. Grid sizes are $\Delta x = \Delta y = 2$ km and $\nu = 5$ m^2 s^{-1}. Boundary conditions are as in Figure 1.

Figure 3. As in Figure 2 with $\tau^{oy} = -10^{-4}$ m^2 s^{-2} applied everywhere except near the southern boundary, where τ^{oy} varies linearly to zero from $y = 100$ to 50 km, and is zero for $y < 50$ km.

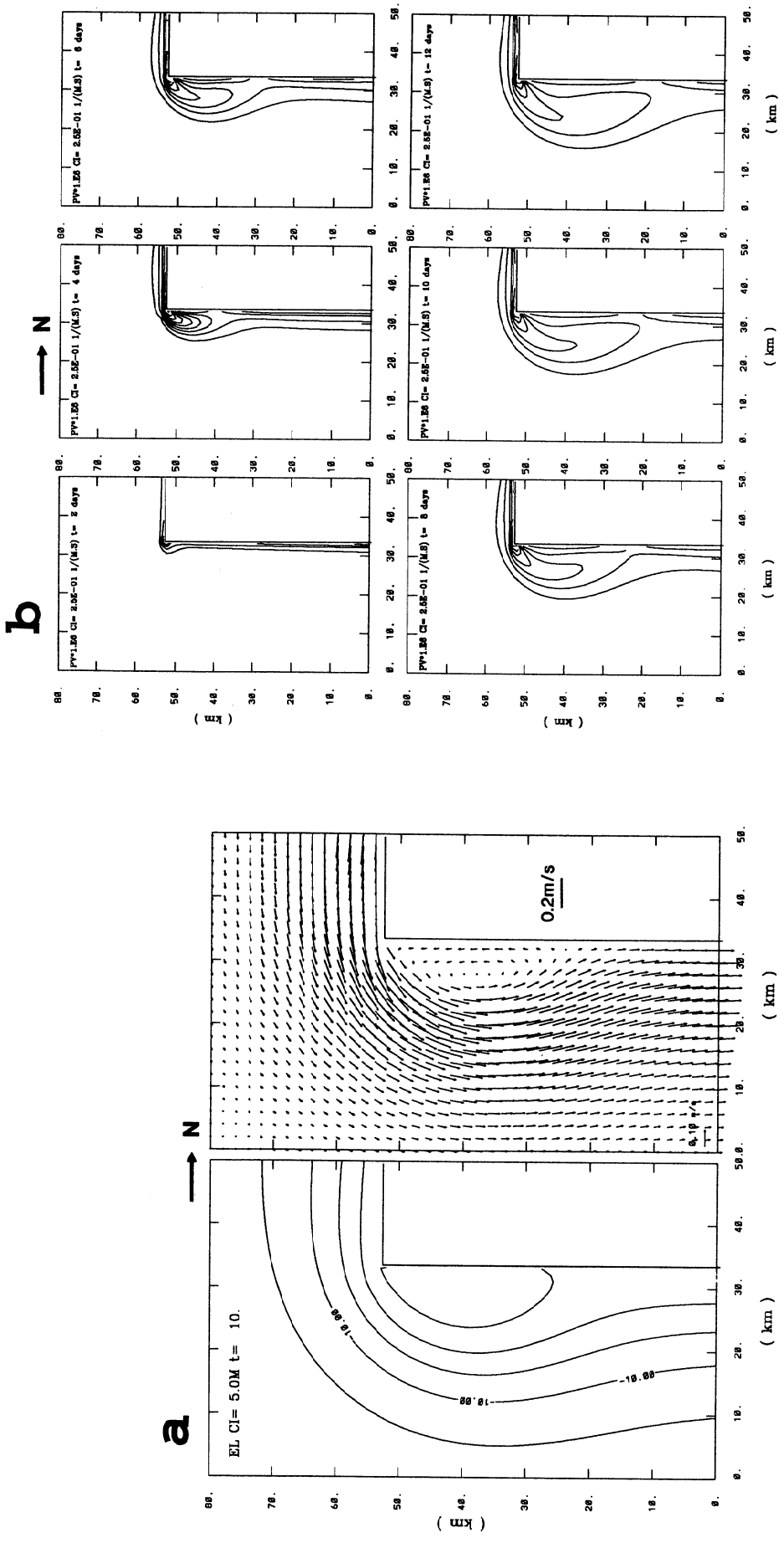

Figure 4. (a) Modeled layer anomaly (CI = 5 m; label is −10 m, i.e., decreased layer depth) and vectors in a subdomain of Figure 2 that focuses on the channel only, with $\Delta x = \Delta y = 1$ km and $\nu = 40$ m^2/s ($R_e = 250$); (b) time sequence of the potential vorticity (CI = 2.5×10^{-7} 1/(meters × second)) showing "steady" state by day 10. The subdomain size is 75 km × 150 km, but only a portion of it is shown from $x = 15$ to 65 km and $y = 47$ to 127 km; note that north is now model's positive x direction.

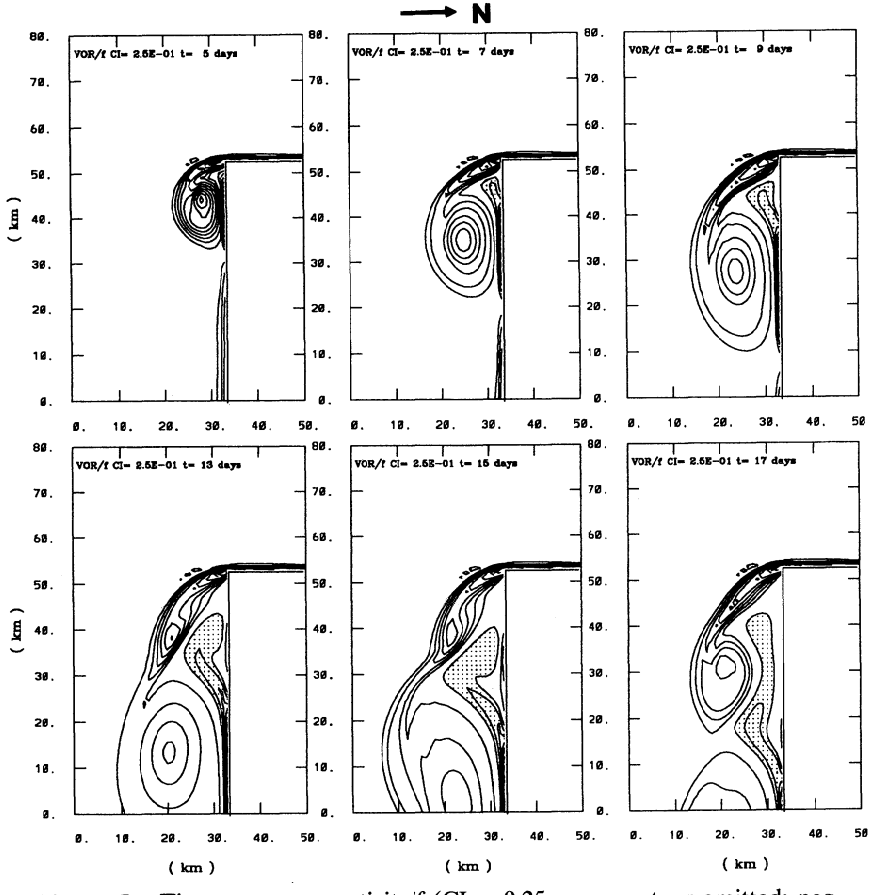

Figure 5. Time sequence vorticity/f (CI = 0.25; zero contour omitted; negative region is stippled) for the case with zero Coriolis, showing drifting of eddy into the channel, and formation of a new eddy at day 17 (R_e = 1000).

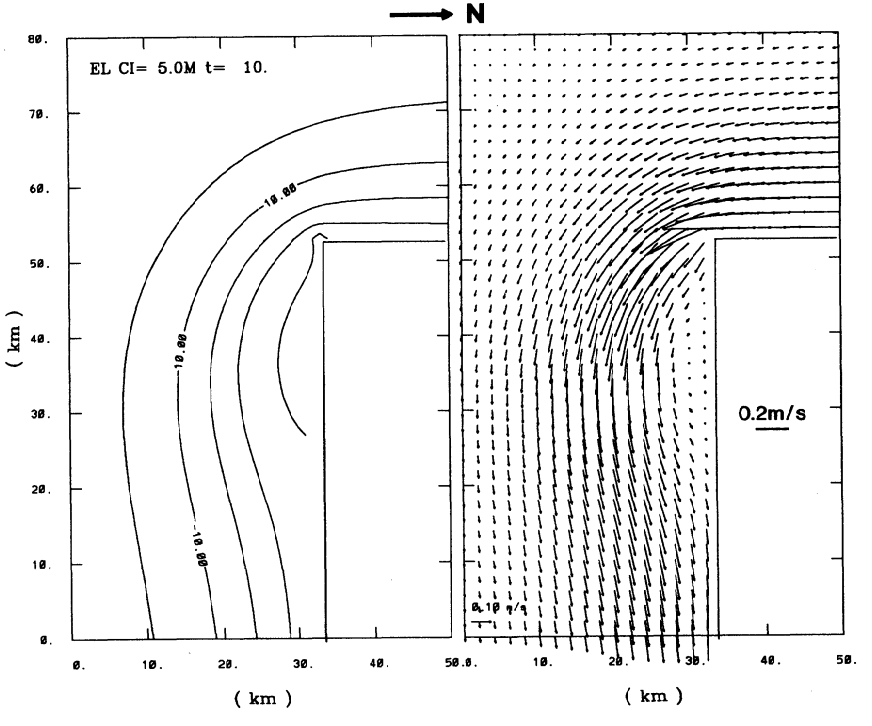

Figure 6. Same as Figure 4a for a near free-slip condition at the corner, showing a weakened cyclone.

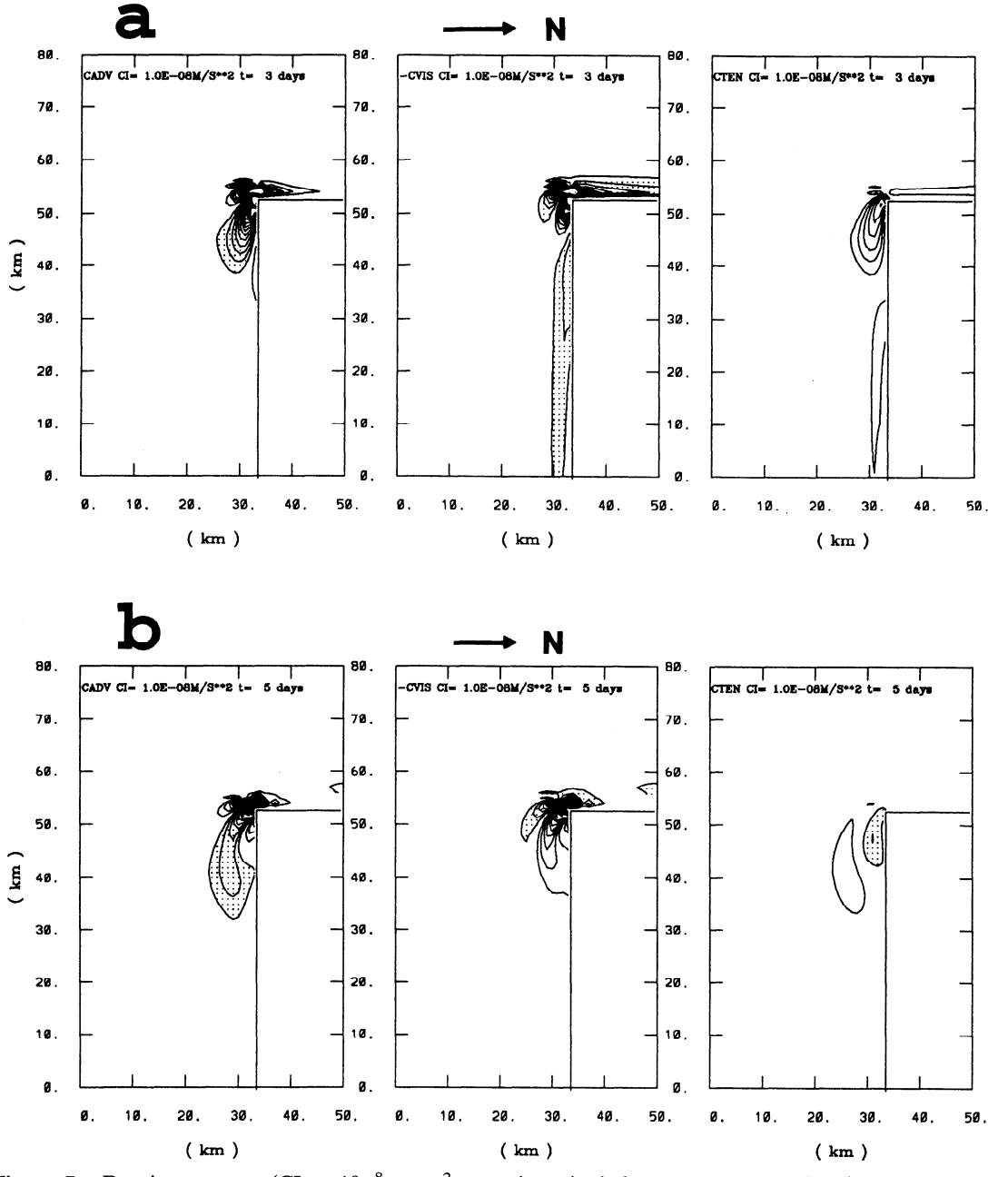

Figure 7. Dominant terms (CI = 10^{-8} m s^{-2}, negative stippled, zero contour omitted) in the vorticity balance for the case shown in Figure 4: (left) advection, (middle) viscous (negative means production of cyclonic vorticity), and (right) tendency for (a) t = 3 days and (b) t = 5 days.

be directly applied to evaluate the wall shear stress terms in (1b). By decreasing "R" I determined a lower limit equal to 0.025 m, below which the model became unstable. Figure 6 shows that with this value of R, the cyclone is nearly eliminated.

The role of advection is examined by evaluating terms in the vorticity equation (curl of (1b)). The primary balance is between the tendency $\partial h\varsigma/\partial t$ (T), advection (A), and viscous (V) terms at early times (Figure 7a) and between A and V at later stages (Figure 7b). The figures also show that vorticity production at the corner dominates that along the straight walls.

3.1. Sensitivity to Viscosity

Reducing ν from 40 (Figure 4) to 20 m^2 s^{-1} (Reynolds number $R_e = v_oL/\nu$ = 250 and 500, where L = 50 km, the channel width) increases the near-wall velocity and hence the corner vorticity and its advection into the channel, resulting in a stronger cyclone (Figures 8a and 8b). The basic mechanism of vorticity generation and advection remains unchanged. At even higher $R_e = v_oL/\nu$ = 1000 and 2000 (not shown), the cyclone's out-channel (i.e., against the free stream) self-advection component (due to image effect with the channel wall) becomes sufficiently strong to balance the in-channel advection of the free stream, so that the cyclone is positioned nearer the corner (Figure 8a, R_e = 1000 case).

3.2. Sensitivity to Rossby Number

The Rossby number $\varepsilon = v_o/fL$ is doubled from 0.05 (Figures 4 and 8) to 0.1 by using v_o = 0.4 m s^{-1} and R_e = 250,

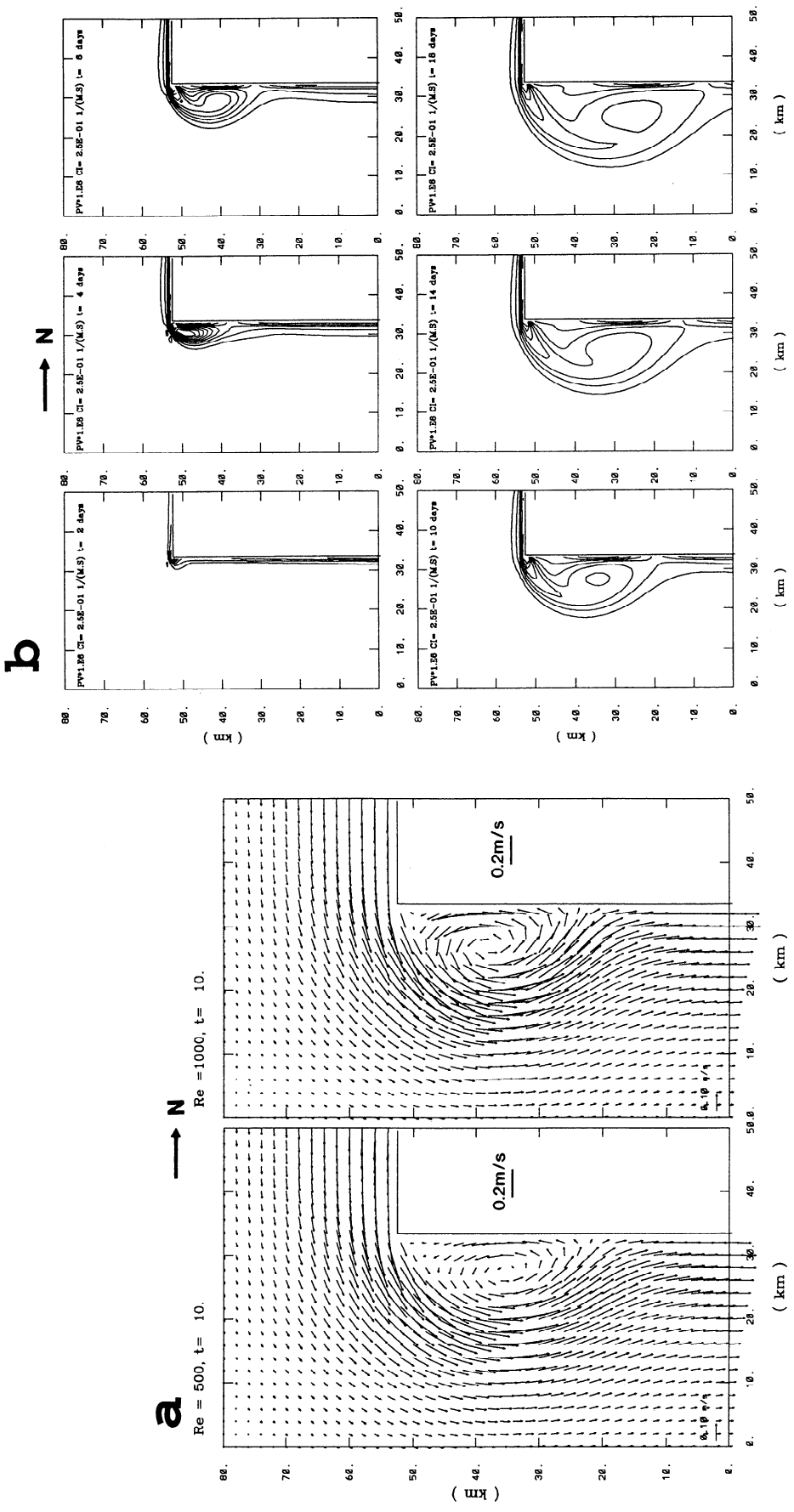

Figure 8. (a) Vectors for $R_e = 500$ and 1000 (compare the $R_e = 250$ case of Figure 4a); (b) time sequence of potential vorticity (CI = 2.5×10^{-7} 1/(meters $\times$ second)) for the $R_e = 500$ case showing drifting of cyclone into the channel (compare the zero Coriolis case of Figure 5).

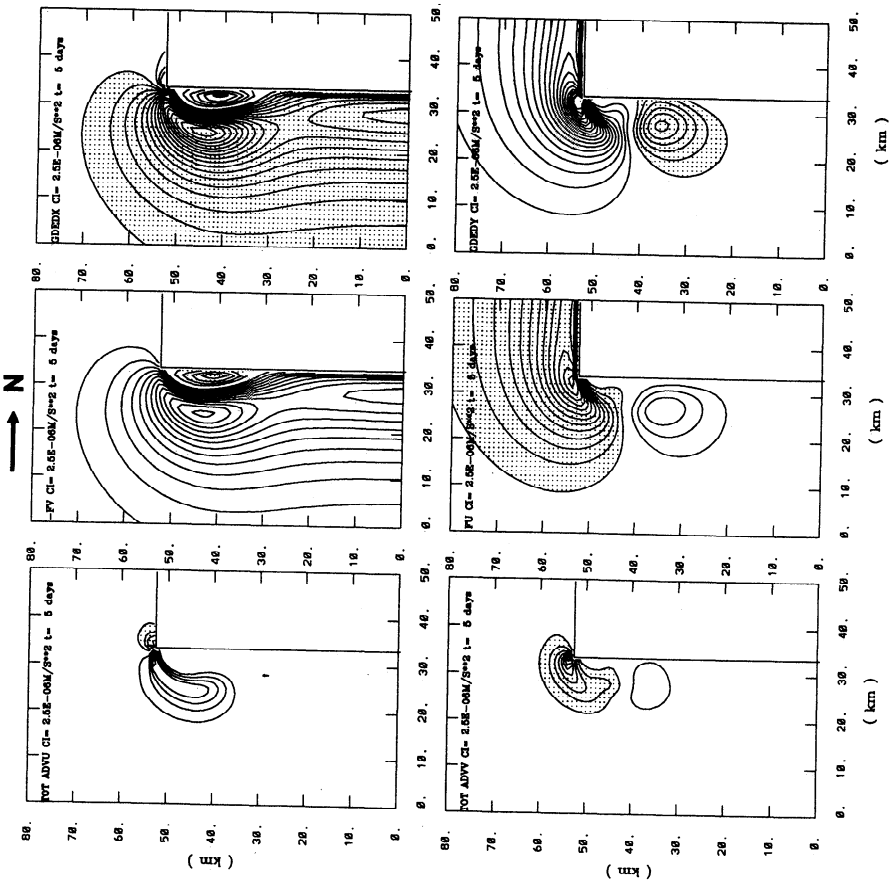

Figure 10. The three dominant terms (CI = 2.5×10^{-6} m s^{-2}, negative values stippled, zero contour omitted) in the (top) x and (bottom) y momentum equations: (left) advection, (middle) Coriolis, and (right) pressure gradient (R_e = 500, ε = 0.05).

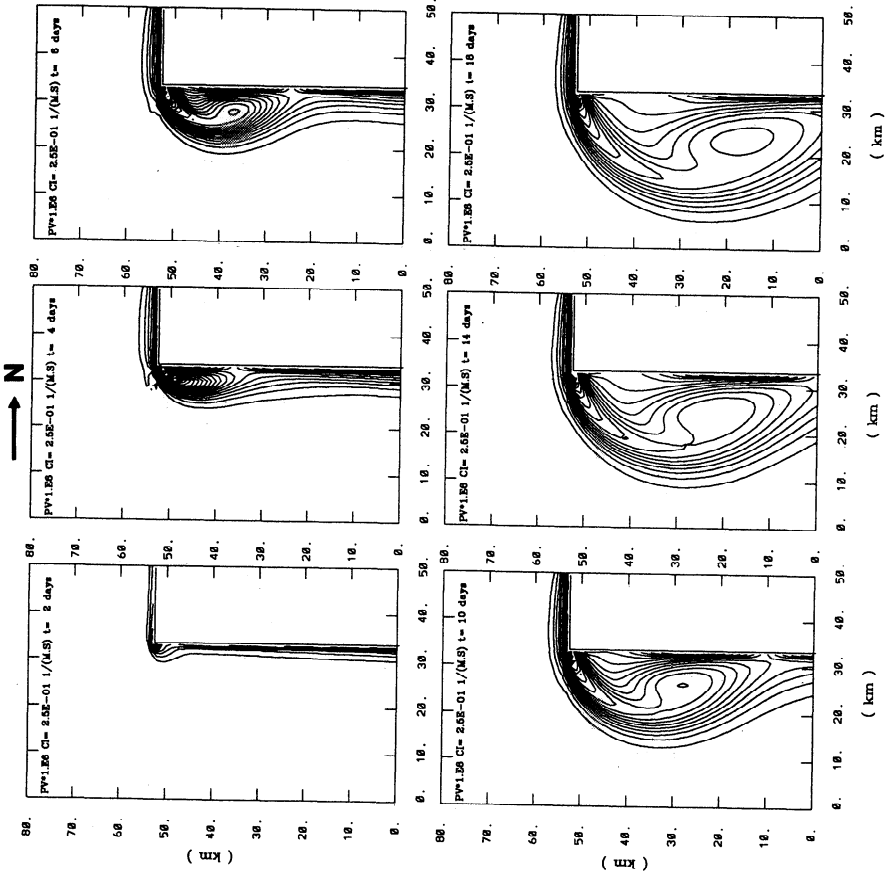

Figure 9. Same as Figure 8b for doubled Rossby number ε = 0.1, showing deeper penetration of eddy in the channel.

500, 1000, and 2000. Figure 9 shows the case with $R_e = 500$ and can be compared with Figure 8b. The cyclone is advected further into the channel at larger ε. In the limit of $\varepsilon \gg 1$ one expects the eddy-shedding regime of Figure 5.

3.3. Momentum Balance

Figure 10 gives three dominant terms in the x and y momentum equations. Away from the corner the balance is nearly geostrophic. At the corner the pressure gradients are balanced by Coriolis (65%) and centrifugal acceleration (represented by the nonlinear momentum advection terms; 35%).

3.4. Sensitivity to Grid Size

The case with $R_e = 500$ and $\varepsilon = 0.05$ was repeated with $\Delta x = \Delta y = 8$, 4, 2, and 0.5 km. The solutions for the two coarsest grids differ from the others (Table 1). The reason is because the boundary layer thickness $\delta \sim L/R_e^{1/2} \sim 2$ km [*Batchelor*, 1967] cannot be resolved at the coarser grids.

3.5. Free-Slip or No-Slip?

The above process depends on the no-slip condition and would apply in a laboratory experiment with real fluids. When modeling the real ocean with fine grid sizes as used here, the no-slip condition would also be more appropriate, except that the model takes no account of the friction associated with bottom shoaling on the continental shelf. However, off California with strong stratification and steep topography, friction is secondary. The following section shows that the same eddy-generation mechanism exists in a more complete model with topography.

4. A 3-D Model With Topography

The three-dimensional, primitive-equation, nested-grid model (Figure 11; see *Oey and Chen* [1992] for details of the model equation and formulation) is used. The fluid is initially at rest, salinity $S = 35$ practical salinity units (psu), and its temperature (degrees Celsius)

$$T(z) = 18 \qquad 0 > z > -25 \text{ m}$$

$$T(z) = 18 - 10\{1 - \exp[(z + 25)/75]\}$$

$$- 6\{1 - \exp[(z + 25)/500]\} \qquad -25 > z > -D$$

where $D(x, y)$ is the water depth. This profile is after *McCreary et al.* [1987] and results in a strong near-surface pycnocline similar to that observed off California. The horizontal viscosity and diffusivity coefficients are based on Smagorinsky's formulation [*Oey and Chen*, 1992] and range from 5 to 40 $m^2 s^{-1}$. A quadratic bottom friction is used with constant coefficient $C_d = 2.5 \times 10^{-3}$. The boundary conditions are no slip and no mass flux at coast, *Orlanski*'s [1976] radiation (with Doppler-shifted phase speeds; otherwise, solution became unstable at north) across the northern and western open boundaries, and zero normal gradients across the southern boundary. A negative wind stress ($\tau^{oy} = -10^{-4}$ $m^2 s^{-2}$) is then applied (increased to the full magnitude over two inertial periods) over the entire domain, except for a 100-km region near the northern boundary where τ^{oy} is linearly decreased to zero. Figure 12 shows the results over the full domain at $t = 24$ days, when an upwelling front and the associated coastal jet are established. An anticyclone/cyclone pair is formed as the jet leaves Point Conception. The seaward anticyclone is caused by the veering of jet due to Coriolis (compare Figure 2), while the cyclone (which extends to about $z = -100$ m) in the western SBC is formed through viscous production and advection of vorticity around the bend. Figure 13 shows details in the high-resolution nest in the channel, from which one sees also the persistence of the cyclone through $t = 41$ days. Thus the basic mechanism of eddy shedding remains valid when realistic topography is used.

A number of tests were conducted: (1) vertical levels = 31

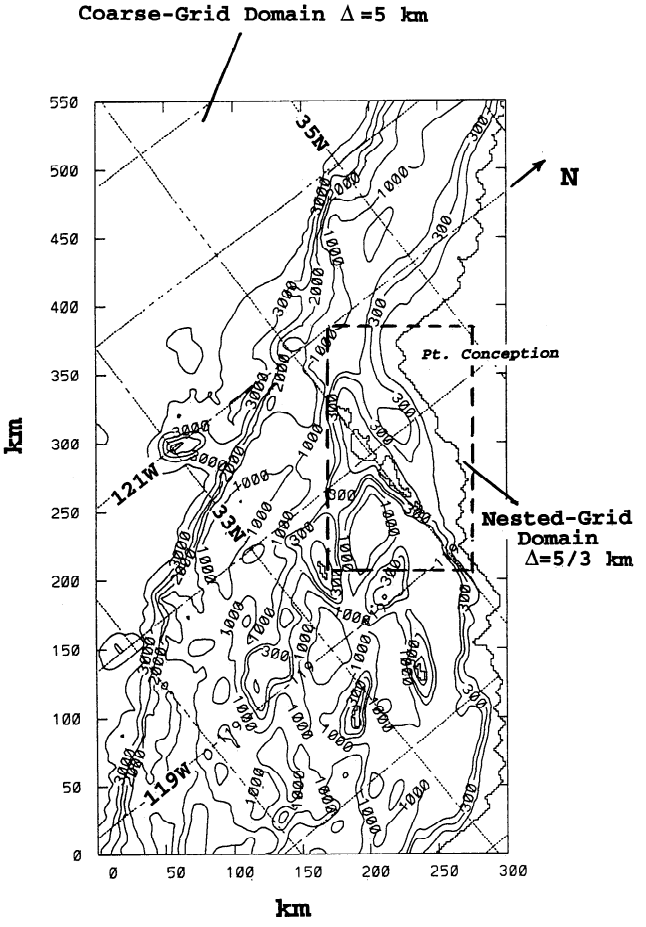

Figure 11. The coarse ($\Delta x = \Delta y = 5$ km) and nested grid ($\Delta x = \Delta y = 5/3$ km) domains and topography (meters; digitized from direct National Ocean Service casts; courtesy of Jim Herring) used in the three-dimensional (3-D) model. The number of vertical sigma levels is 11.

Table 1. Sensitivity of Maximum Currents of Cyclone (at Day 20) to Grid Size for the Case Shown in Figure 8a

Grid Size, km	In-Channel, cm s^{-1}	Out-Channel, cm s^{-1}
8	−4	0.6
4	−11	4.7
2	−18.1	9.5
1	−21.3	11.2
0.5	−21.2	12.3

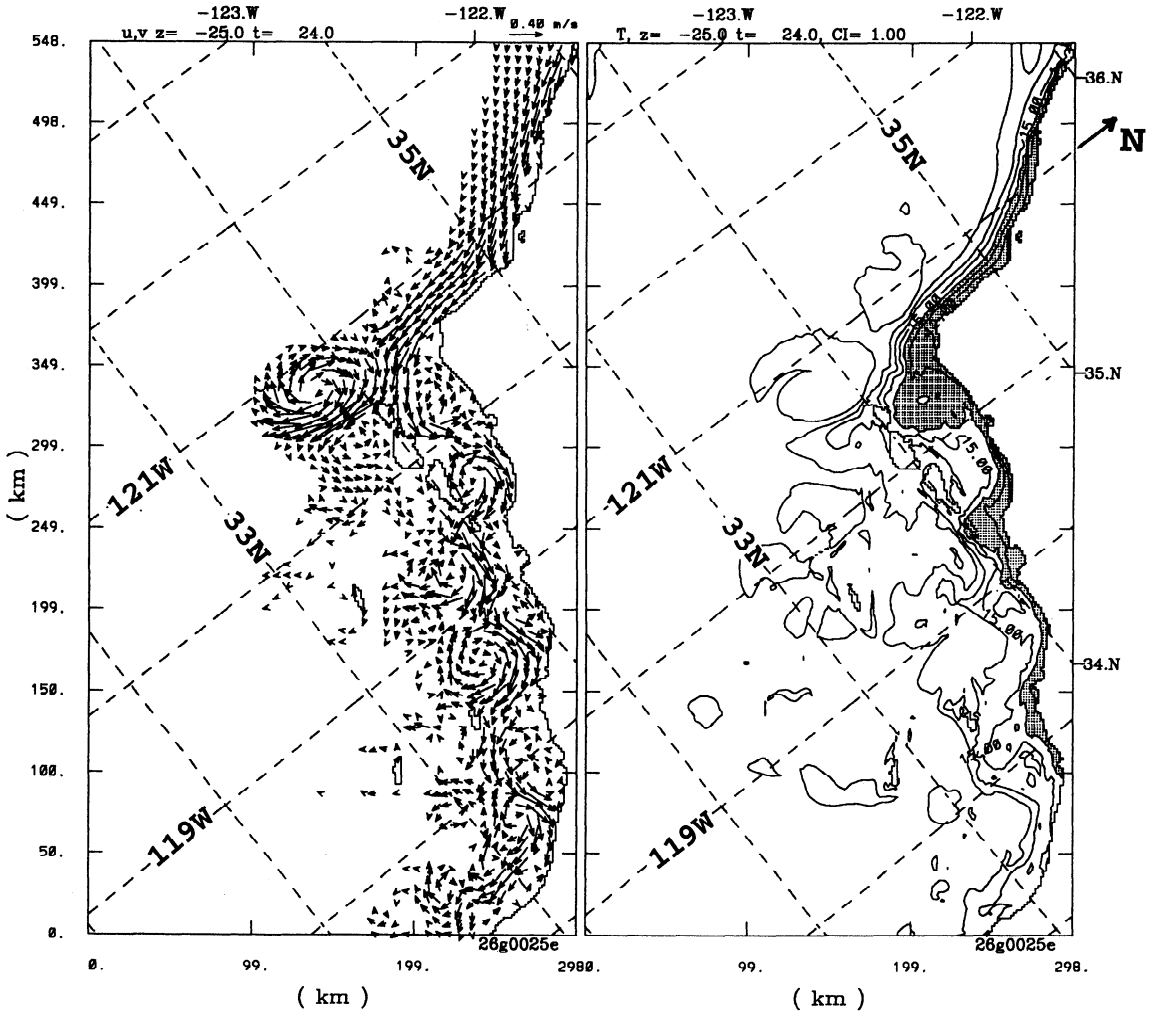

Figure 12. The coarse-grid three-dimensional model results at $t = 24$ days and $z = -25$ m: (left) velocity vectors and (right) temperature (CI = 1°C; figure is stippled where $T < 14$°C).

instead of 11; (2) horizontal grids are uniformly coarse ($\Delta x = \Delta y = 5$ km; no nesting) and (3) uniformly fine ($\Delta x = \Delta y = 5/3$ km; no nesting); (4) horizontal viscosity and diffusivity = 20 m^2 s^{-1}, a constant; (5) beta effect; (6) bottom friction coefficient reduced to $C_d = 6.25 \times 10^{-4}$; and (7) no wind forcing. Tests 1, 3, and 4 gave similar results to those shown in Figures 12 and 13 (base case). Beta (test 5) has negligible effects at early stages of cyclone development. After about 30 days, westward propagating Rossby waves slow down the eastward advection of the cyclone into the channel. The cyclone strengthens in test 6; otherwise, the results are similar to the base case. Test 2 gave no cyclonic gyre in the western SBC and again demonstrates the importance of good resolution. Experiment 7 gave a maximum speed of a few millimeters per second at the end of a 50-day integration and ensured that the pressure-gradient error in sigma coordinate remained negligible.

The idea of eddy shedding behind a bluff body has been applied to homogeneous tidal flows in shallow waters [*Tee*, 1976; *Signell and Geyer*, 1991, and references therein]. A common thread that ties these and the present studies is that the shed-off eddy depends on the vorticity generated around the bend (headland), a mechanism demonstrated in the previous section; the eddy was nullified when a free-slip condition that is a function of the radius of curvature of the bend was imposed. Signell and Geyer suggested that the vorticity produced by the curl of bottom friction due to near-coast shoaling dominates that produced by viscosity and that the latter mimics the former in a grid that is too coarse to resolve shoaling. Thus how the boundary vorticity is generated is not the main issue here, provided that it exists.

The present calculation differs from the tidal problem in two aspects (apart from different time dependencies). First, because rotation is important, the shed-off eddy tends to adjust geostrophically behind the bend (compare Figures 8b, 9, and 5 for increasing Rossby number). This, coupled with the wall-image effect (i.e., mirror image of the eddy in the wall to satisfy zero normal flow condition at the wall; Figure 8), can provide a mechanism by which the cyclonic gyre in the western Santa Barbara Channel can remain persistent. Second, test 6 shows that bottom friction is relatively unimportant because of the

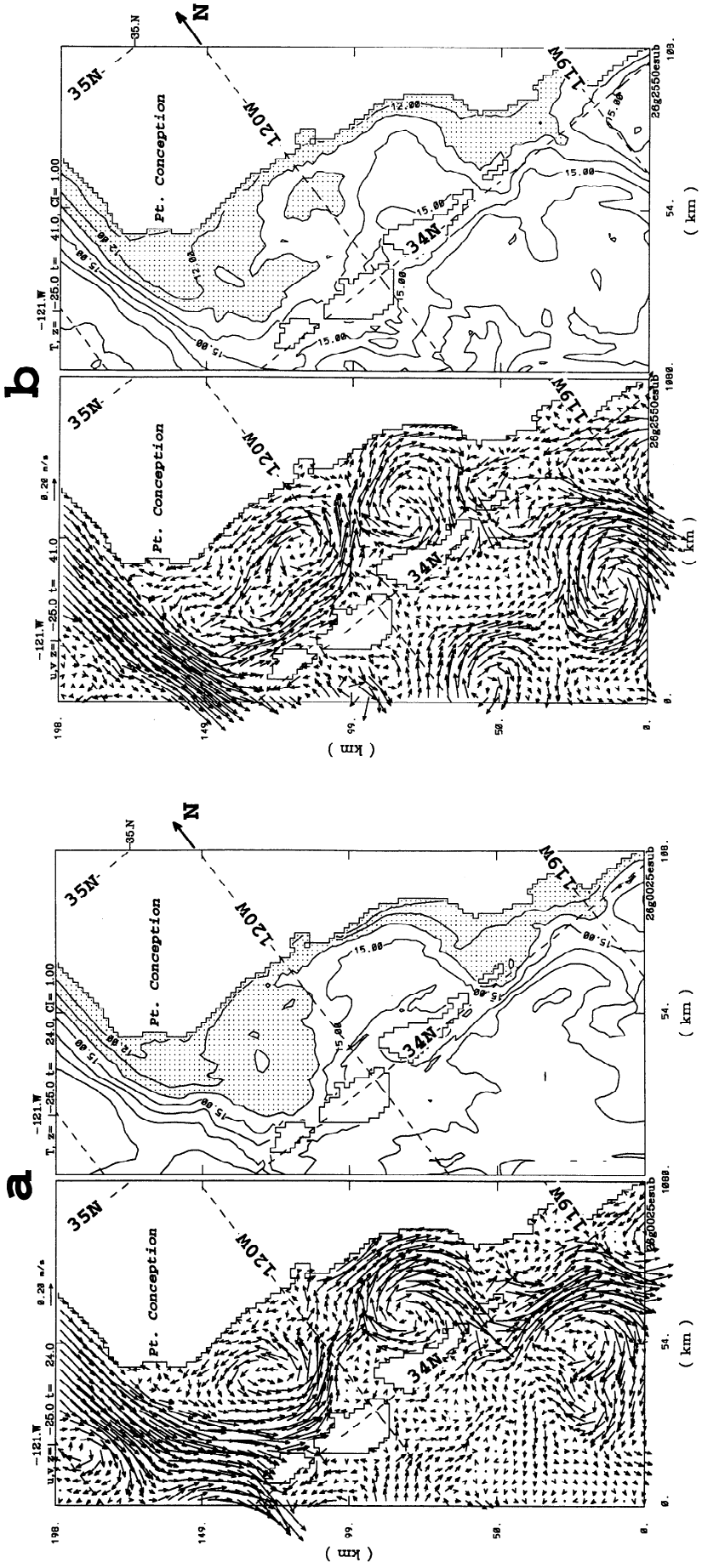

Figure 13. The three-dimensional model results inside the nest at $z = -25$ m and (a) $t = 24$ days and (b) $t = 41$ days: (left) velocity vectors and (right) temperature (CI = 1°C; figure is stippled where $T < 14$°C).

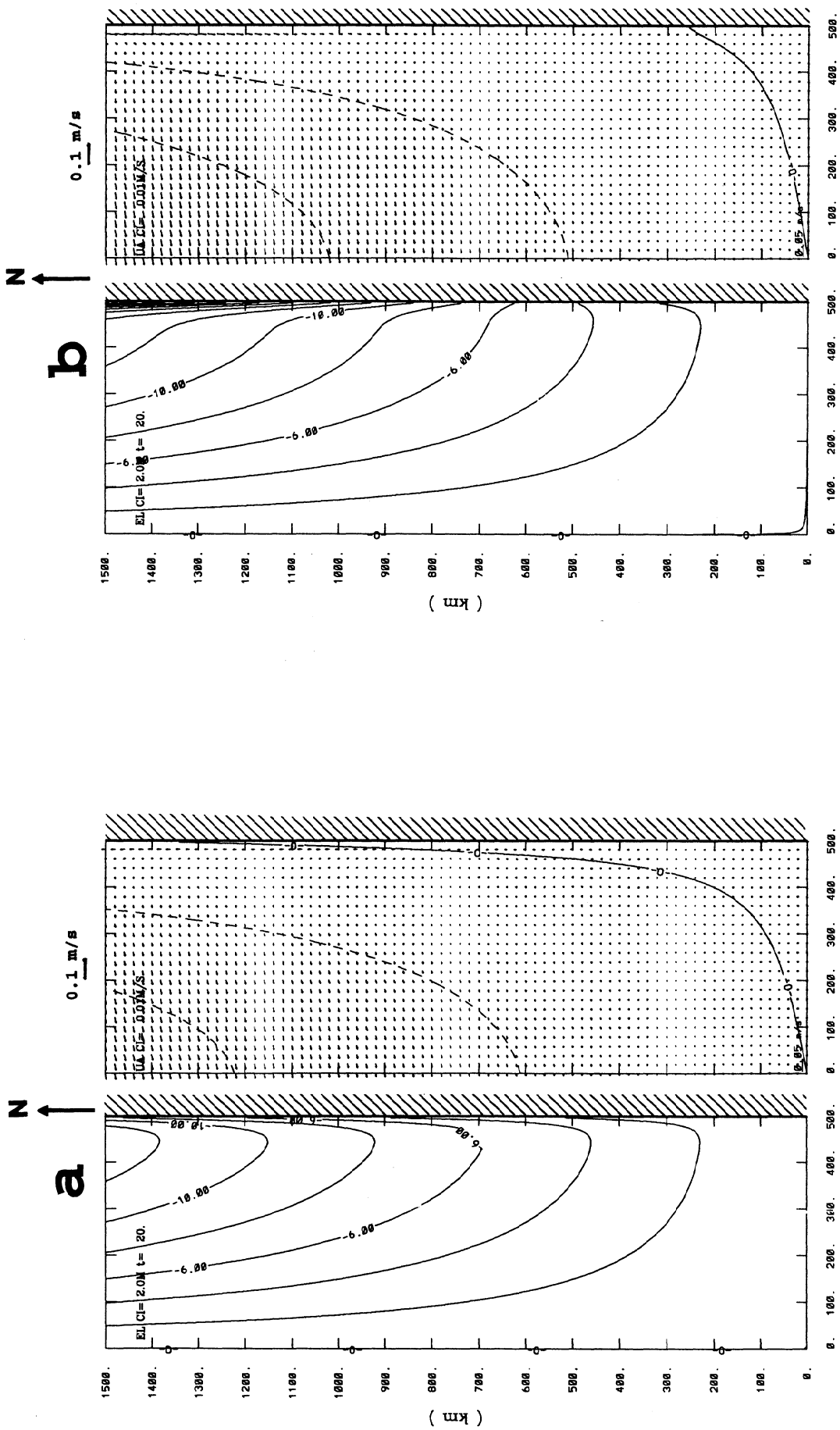

Figure 14. Linear model solution for (a) $\gamma = 0$ (curl only) and (b) $\gamma = 0.2$ (curl and wind at coast): (left) layer anomaly (CI = 2 m) and (right) vectors. Here $\tau_o = 0.2$ N/m^2. Superimposed on vectors are also contours of cross-shore velocity (CI = 1 cm/s; dashed lines are negative values).

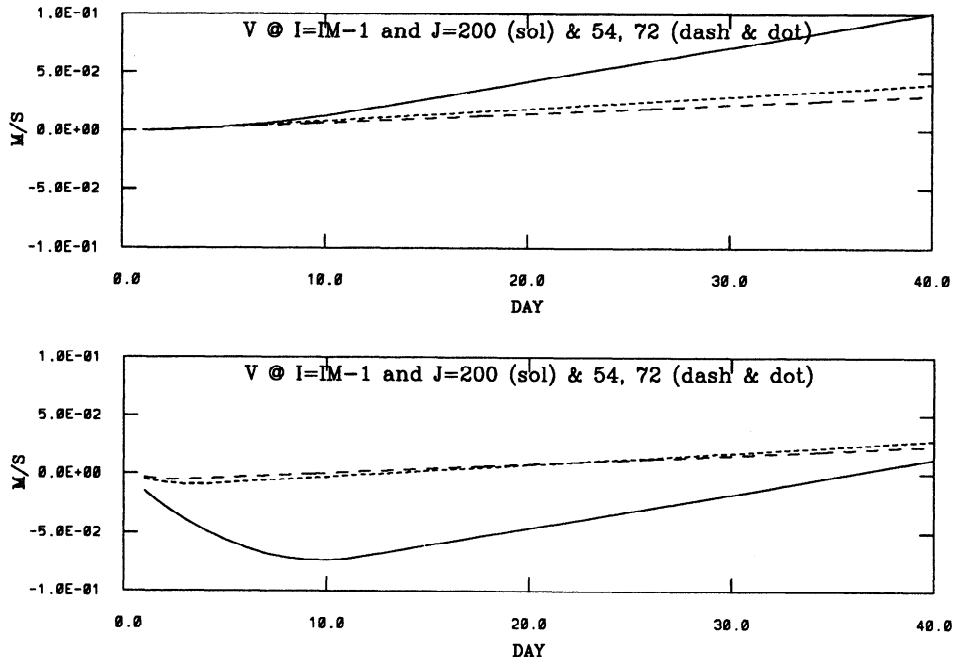

Figure 15. Alongshore currents one grid away from coast for the (top) $\gamma = 0$ case and (bottom) $\gamma = 0.2$ case: solid lines are for $y = 1000$ km, dotted lines are for $y = 360$ km, and dashed lines are for $y = 270$ km. The $\gamma = 0$ case is dominated by northward currents, while the $\gamma = 0.2$ case consists of the direct wind-driven response (southward current) at early stage, turning northward as the curl dominates with time.

strong stratification and a topography that drops off steeply offshore and it is small because of the weak bottom flow.

5. The SBC Cyclone: Effects of Wind Stress and Its Curl

In the Southern California Bight, wind generally decreases in strength south of Point Conception especially near the coast, and wind curl is large [*Hickey*, 1979]. The wind weakens further to the south off Baja California. Since the coastal current that produces the SBC cyclone is forced from the south, it is of interest to examine how the near-coast currents respond to a combined wind and wind-curl forcing. (When revising the manuscript, I came across the paper by *McCreary et al.* [1987], which contains some of the conclusions derived herein. Although there are differences (time dependency, for example), the present analysis can nevertheless be considered as a simple reduction of their more complete model.)

The effect can be understood via linear dynamics:

$$\eta_t + H\nabla \cdot (\mathbf{u}) = 0 \tag{2a}$$

$$\partial(\mathbf{u})/\partial t + f\mathbf{k} \times \mathbf{u} = -g'\nabla\eta + \tau^o/H \tag{2b}$$

where $\eta = h - H$, the layer anomaly. An equation for $E = f\eta/H$ can be derived:

$$(\partial^2/\partial t^2 + f^2 - C^2\nabla^2)E = -(f/H)(ft\nabla \times \tau^o + \nabla \cdot \tau^o) \tag{3}$$

The straight coast is along $x = 0$, so that ocean occupies $x < 0$ and positive y is north. Wind is alongshore, turned on at $t = 0^+$ in region $y > 0$, then kept time independent, $\tau^o = (0, \tau^y)$, and assuming also $\partial^2/\partial t^2 \ll f^2$ and $\partial^2/\partial y^2 \ll \partial^2/\partial x^2$. Equation (3) becomes

$$(f^2 - C^2\partial^2/\partial x^2)E = -(f/H)ft\partial\tau^y/\partial x \tag{4}$$

This equation is also consistent with the assumption that the cross-shore momentum balance is geostrophic: $fv = g'\partial\eta/\partial x$. A solution is obtained with the following wind

$$\tau^y(x, y) = \tau_o\beta y(\sin \alpha x - \gamma), \tag{5}$$

where $\alpha = \pi/(2L_x)$, $\beta = 1/L_y$, τ_o is the wind stress value, and γ is a constant proportional to wind at the coast. For convenience the domain is bounded by $0 < y < L_y$ and $-L_x < x < 0$ ($L_x \gg C/f$), so that the wind varies linearly from zero at $y = 0$ (Baja California) to some value at $y = L_y$ (central California) and also from $-\tau_o\beta y\gamma$ at the coast ($x = 0$) to a maximum $-\tau_o\beta y(1 + \gamma)$ at $x = -L_x$. Thus

$$E(x, y, t) = A(y, t)e^{fx/C} + (a_2\alpha/\beta)[ft\beta y \cos \alpha x + O(L_x/L_y)] \tag{6}$$

where $a_2 = -f\tau_o\beta/[H(f^2 + C^2\alpha^2)]$. The neglected term is $O(\gamma\tau_o\beta/Hf) \approx 10^{-8}$ s^{-1}, or $\eta \sim O$ (centimeters). The cosine term defines the far field and is supplemented by the homogeneous term in order to satisfy the boundary condition $u = 0$ at $x = 0$ [*Gill*, 1982],

$$(\partial/\partial t + C\partial/\partial y)A = (-Ca_2\alpha f)t + f\tau^y(0, y)/(CH), \tag{7}$$

a forced Kelvin wave equation. The first forcing term is proportional to the wind curl at the coast and is caused by the

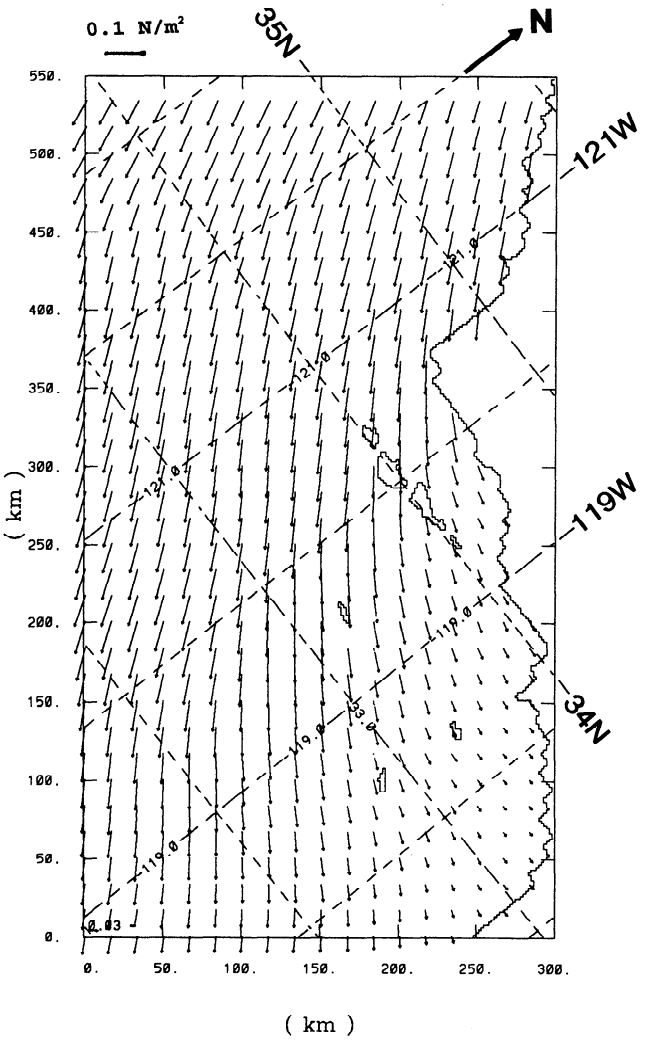

Figure 16. California Cooperative Oceanic Fisheries Investigation (CalCOFI) spring wind stress (courtesy of Clinton Winant). Maximum vector is 0.16 N m^{-2}.

alongshore gradient in the wind curl or, since wind curl affects the layer thickness, by the alongshore pressure gradient imposed by the far field. In the Southern California Bight the (positive) wind curl weakens, and hence pressure strengthens, southward. This contributes to a layer thickening in the forced Kelvin wave ((7); note that $a_2 < 0$), hence a northward coastal current. This current is opposite to that induced by (negative) wind stress at the coast (the second forcing term in (7)), which contributes to layer thinning. A solution to (7) that satisfies $A(y, 0) = A(0, t) = 0$ is

$$A(y, t) = -C\alpha f a_2 t^2/2 - (a_1 f^2/C)(y - Ct/2)t \quad (8a)$$

$$y > Ct$$

$$A(y, t) = -\alpha f a_2 y(2t - y/C)/2 - (a_1 f^2/C^2)y^2/2 \quad (8b)$$

$$y < Ct$$

where $a_1 = \tau_o \beta \gamma/(Hf)$. The complete solution is given by (6) and (8), from which $v = (g' \partial\eta/\partial x)/f$, and u is obtained from either the continuity or the y momentum equation.

Figures 14 and 15 give results for $\gamma = 0$ (curl only) (Figures 14a and 15a) and $\gamma = 0.2$ (curl and wind at coast) (Figures 14b and 15b). In the former, flow is forced toward the coast in the south by the alongshore pressure gradient that overcomes the wind-driven offshore transport and feeds the northward flowing coastal current. The latter shows a southward coastal current especially in the northern region, the wind-forced Kelvin wave solution. In time this is overwhelmed by the curl-forced solution, which begins first in the south and travels up the coast. The time when the two effects balance can be estimated by setting the right-handside of (8b) to zero:

$$t_c \approx (\gamma f/2\alpha C^2)y \approx 10\gamma y/C^2 \quad (9)$$

assuming a cross-shore wind-curl scale of about 200 km. At the SBC location ($y \approx 1200$ km), with $\gamma \approx 0.2$ and $C \approx 1$ m s^{-1}, $t_c \sim 30$ days. Thus following an eastward channel flow caused by the wind-forced solution (superimposed by the cyclone as described previously), the circulation in the channel enters a different dynamical regime, in time $O(t_c)$, in which the large-scale wind stress curl in the Southern California Bight becomes important.

Several calculations with the numerical model (same domain as Figure 14) of the previous section were conducted with other types of wind distributions: linear, step function, Gaussian, and more complicated sinusoids. The above conclusion about wind and wind-curl interactions remains valid.

As an example of how the two effects interact, the model of Figure 1 was run with California Cooperative Oceanic Fisheries Investigations (CalCOFI) spring wind forcing (Figure 16; courtesy of Clinton Winant, Scripps Institution of Oceanography). Figure 17 shows the results at two times: an early stage ($t = 20$ days), when the direct-wind forced solution prevails and a cyclone is formed, and a later stage ($t = 36$ days) when the curl part begins to dominate and the westward current along the north coast strengthens, while the eastward flow along the channel islands weakens.

6. Conclusions

Additional experiments indicate that new eddies are generated by time-dependent ambient currents through continual vorticity production. This suggests a plausible mechanism for persistent eddy features in the SBC forced by synoptic wind field. Over a longer timescale of 0 (months) the eddies are embedded in the curl-forced gyre of the Southern California Bight, and a quasi-permanent recirculation, with stronger outchannel current in the north channel than the in-channel current in the south, would result (Figure 17). While data [e.g., *Brink and Muench*, 1986] appear to support this, a more complete model and analysis of observations are required.

The three-dimensional model shows that the cyclone-formation mechanism through viscous production and advection of vorticity around a bend is robust and that for longer time ($t > 30$ days), topography and beta become important. Topography tends to strengthen the cyclone as near-bottom flow develops cyclonically around the channel, an extension of the coastal undercurrent that flows anticyclonically from the southern coastline of the islands chain. Beta tends to weaken the cyclone as disturbances emanate westward from west of the channel. These and other three-dimensional results (instability and meanders) will be the subject of a follow-up paper.

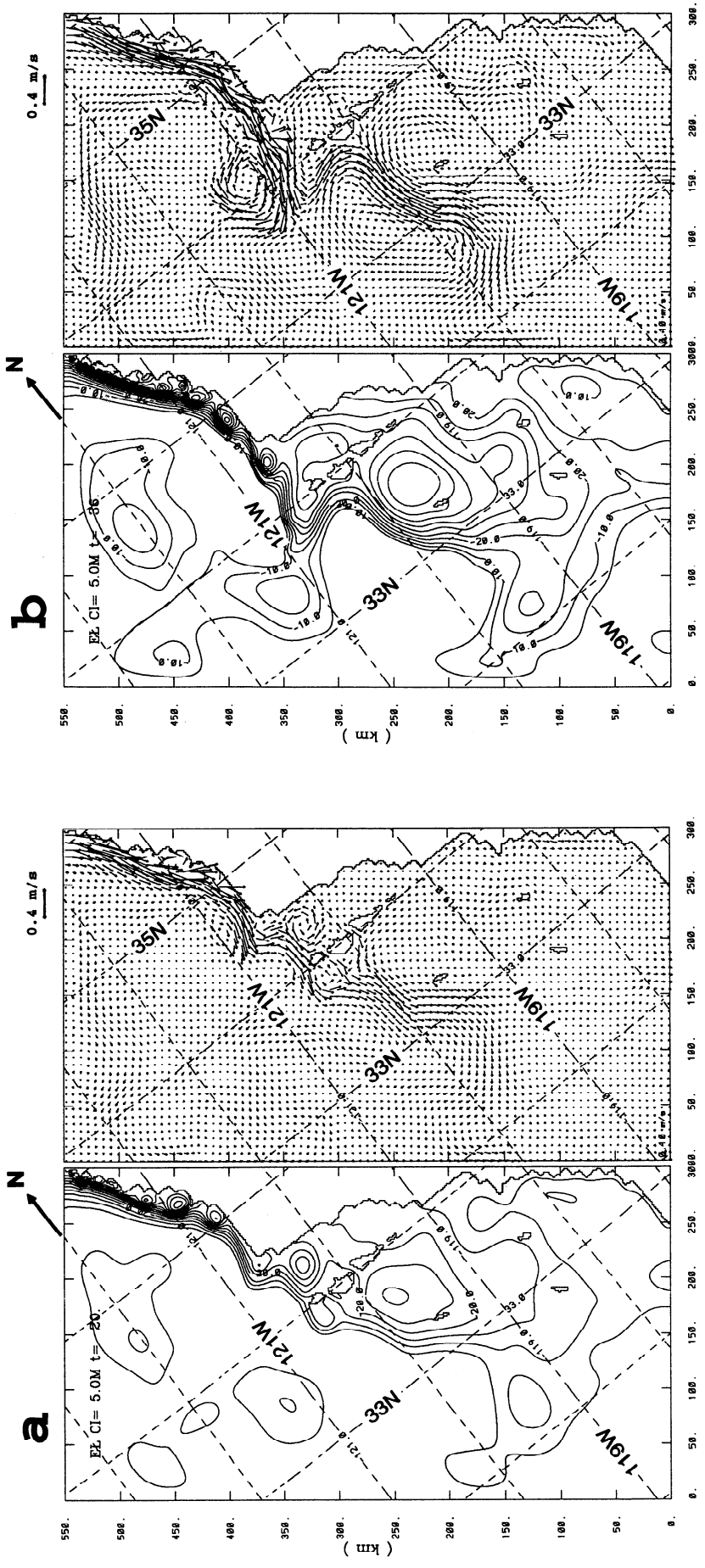

Figure 17. The model layer anomaly (CI = 5 m, plotted values are negative) and vectors at (a) $t = 20$ days and (b) $t = 36$ days, before and after the full establishment of the curl-forced solution. The model is forced by CalCOFI spring wind stress of Figure 16 but is otherwise the same as in Figure 1.

Acknowledgments. I appreciate inputs from John Allen, Patrick Cummins, Dong-Ping Wang, Clinton Winant, and two anonymous reviewers. This work was funded by the Mineral Management Service (COTR, David Browne), via the Scripps Institute of Oceanography, and the Office of Naval Research (Program Manager, Manuel Fiadeiro). Computing was performed at the Pittsburgh Supercomputing Center and the National Center for Supercomputing Applications, Illinois.

References

Batchelor, G. K., *An Introduction to Fluid Dynamics*, 615 pp., Cambridge Univ. Press, New York, 1967.

Brink, K. H., and R. D. Muench, Circulation in the Point Conception-Santa Barbara Channel region, *J. Geophys. Res.*, *91*, 877–895, 1986.

Gill, A. E., *Atmosphere-Ocean Dynamics*, 662 pp., Academic, San Diego, Calif., 1982.

Hickey, B. M., The California Current System—Hypotheses and facts, *Prog. Oceanogr.*, *8*, 191–279, 1979.

Holloway, G., and P. Rhines, Angular momenta of modeled ocean gyres, *J. Geophys. Res.*, *96*, 843–846, 1991.

Lagerloef, G. S. E., and R. L. Bernstein, Empirical orthogonal function analysis of advanced very high resolution radiometer surface temperature patterns in Santa Barbara Channel, *J. Geophys. Res.*, *93*, 6863–6873, 1988.

McCreary, J. P., P. K. Kundu, and S.-Y. Chao, On the dynamics of the California Current system, *J. Mar. Res.*, *45*, 1–32, 1987.

Narimousa, S., and T. Maxworthy, Application of a laboratory model to the interpretation of satellite and field observations of coastal upwelling, *Dyn. Atmos. Oceans*, *13*, 1–46, 1989.

Oey, L.-Y., and P. Chen, A nested-grid model simulation of the Norwegian coastal current, *J. Geophys. Res.*, *97*, 20,063–20,086, 1992.

Orlanski, I., A simple boundary condition for unbounded hyperbolic flows, *J. Comput. Phys.*, *21*, 251–269, 1976.

Roache, P. J., *Computational Fluid Dynamics*, 446 pp., Hermosa, Albuquerque, N. M., 1972.

Signell, R. P., and W. R. Geyer, Transient eddy formation around headlands, *J. Geophys. Res.*, *96*, 2561–2575, 1991.

Tee, K. T., Tide-induced residual current, a 2-D nonlinear numerical tidal model, *J. Mar. Res.*, *34*, 603–628, 1976.

L.-Y. Oey, Program in Atmospheric and Oceanic Sciences, Sayre Hall, Forrestal Campus, Princeton University, Princeton, NJ 08544. (e-mail: lyo@kuroshio.princeton.edu)

(Received July 17, 1995; revised December 12, 1995; accepted April 1, 1996.)